INL/JOU-22-66964-Revision-0

Electrical, Thermal, and H2O and CO2 Poisoning Behaviors of PrNi0.5Co0.5O3-d Cathode for Proton Conducting Intermediate Temperature Solid Oxide Fuel Cell

Zhe Cheng, Dong Ding, Wei Tang, Md Shariful Islam Sozal, Suprabha Das , Wenhao Li, Andriy Durygin , Vadym Drozd, Cheng Zhang, Borzooye Jafarizadeh , Chunlei Wang, Arvind Agarwal

Changing the World's Energy Future

Idaho National Laboratory

INL is a U.S. Department of Energy National Laboratory operated by Battelle Energy Alliance, LLC

INL/JOU-22-66964-Revision-0

Electrical, Thermal, and H2O and CO2 Poisoning Behaviors of PrNi0.5Co0.5O3-d Cathode for Proton Conducting Intermediate Temperature Solid Oxide Fuel Cell

Zhe Cheng, Dong Ding, Wei Tang, Md Shariful Islam Sozal, Suprabha Das , Wenhao Li, Andriy Durygin , Vadym Drozd, Cheng Zhang, Borzooye Jafarizadeh , Chunlei Wang, Arvind Agarwal

June 2022

Idaho National Laboratory
Idaho Falls, Idaho 83415

http://www.inl.gov

Prepared for the
U.S. Department of Energy
Under DOE Idaho Operations Office
Contract DE-AC07-05ID14517, NSF

Electrical, Thermal, and H_2O and CO_2 Poisoning Behaviors of $PrNi_{0.5}Co_{0.5}O_{3-\delta}$ Electrode for Intermediate Temperature Protonic Ceramic Electrochemical Cells

Md Shariful Islam Sozal [a,b], Wei Tang [c], Suprabha Das [a,b], Wenhao Li [a,b], Andriy Durygin [b], Vadym Drozd [b], Cheng Zhang [a], Borzooye Jafarizadeh [a,b], Chunlei Wang [a,b], Arvind Agarwal [a], Dong Ding [c*], Zhe Cheng [a,b*]

[a] Department of Mechanical and Materials Engineering, Florida International University, Miami, FL, 33174, USA

[b] Center for the Study of Matter at Extreme Conditions (CeSMEC), Florida International University, Miami, FL, 33199, USA

[c] Energy & Environmental Science and Technology, Idaho National Laboratory, Idaho Falls, ID 83415, USA

*Correspondence: Dr. Dong Ding dong.ding@inl.gov; Dr. Zhe Cheng zhcheng@fiu.edu

Abstract

$PrNi_{0.5}Co_{0.5}O_{3-\delta}$ (PNC) exhibits adequate total electrical conductivity (~300 S/cm at 400-600°C) and moisture has no significant effect on it. The thermal expansion coefficient of PNC is 17.6×10^{-6}/K by dilatometry and 18.43×10^{-6}/K by *in situ* XRD. PNC also demonstrates chemical stability against H_2O and CO_2. However, PNC symmetrical cell over proton-conducting $BaZr_{0.4}Ce_{0.4}Y_{0.1}Yb_{0.1}O_{3-\delta}$ (BZCYYb4411) electrolyte shows significant H_2O and CO_2 poisoning when those are introduced into O_2-N_2 mixture. In comparison, symmetrical cells with PNC electrode over the oxygen ion conducting $Ce_{0.9}Gd_{0.1}O_{2-\delta}$ (GDC) electrolyte show no H_2O and

CO_2 poisoning under similar conditions. It is hypothesized that poisoning from H_2O and CO_2 of the PNC proton conducting symmetrical cell is caused by their adsorption on the BZCYYb4411 electrolyte instead of PNC electrode. Such a hypothesis is supported by the H_2O and CO_2 adsorption behaviors on PNC and BZCYYb4411 powder surfaces, as measured by temperature programmed desorption (TPD).

Keywords: Protonic Ceramic Electrochemical Cells; Oxygen Electrode; Electrochemical Behavior; CO_2; H_2O; Temperature Programmed Desorption

1. Introduction

Intermediate temperature (400-600°C) ceramic electrochemical cells are now considered a potential source for clean power generation (as fuel cells) and electrolytic fuel production (as electrolysis cells).[1,2] For these electrochemical systems, proton conducting oxides are often used as the electrolyte because they have a lower activation energy for ion conduction than oxygen-ion conducting electrolytes and offer higher ionic conductivity at intermediate temperature.[3–8] Comparing with conventional ceramic electrochemical cells, intermediate temperature (400-600°C) protonic ceramic electrochemical cells (IT-PCEC) may offer advantages such as cheaper/easier sealing and interconnect, higher thermodynamic efficiency, no fuel dilution, and decent coking/sulfur resistance.[2,5,7,9,10] Earlier studies have shown that acceptor doped barium zirconium cerium oxides can show very high proton conductivity at intermediate temperature, and one promising example is $BaZr_{0.1}Ce_{0.7}Y_{0.1}Yb_{0.1}O_{3-\delta}$ (BZCYYb1711).[3–5,7,11] However, following studies have shown that BZCYYb1711 still reacts with CO_2 under certain conditions.[12,13] In comparison, recent studies have shown that $BaZr_{0.4}Ce_{0.4}Y_{0.1}Yb_{0.1}O_{3-\delta}$ (BZCYYb4411) is stable against 100% CO_2 and enables high-power density at intermediate

temperatures.[14]

On the other hand, the oxygen reduction reaction and its reverse reaction at the oxygen electrode is often claimed to be the rate-limiting step for IT-PCEC (especially fuel cells) because of slower electrode kinetics at intermediate temperature. For oxygen electrode materials such as $La_{0.6}Sr_{0.4}Co_{0.8}Fe_{0.2}O_3$ (LSCF), electrode reaction happens at the triple phase boundary (TPB) between electrolyte, electrode, and gas at intermediate temperature.[15,16] To enable faster oxygen electrode kinetics for IT-PCEC, some proposed that it would be beneficial to make the whole oxygen electrode surface active by adopting triple conducting electrodes that conduct electron, oxygen ion, and proton (e^-, $V_o^{\cdot\cdot}$, $(OH)_o^{\cdot}$) at the same time.[17,18] Triple conducting oxygen electrodes for IT-PCEC (especially fuel cells) are mostly rare earth or early transition metal doped perovskites (ABO_3) or double perovskites ($A_2BB'O_6$) containing A-site alkaline earth elements such as Ba or Sr. Examples reported in the literature include $BaCe_{0.5}Bi_{0.5}O_{3-\delta}$ (BCB)[19,20], $PrBa_{0.5}Sr_{0.5}Co_2O_{5+\delta}$ (PBSC)[21], $BaZr_{0.5}Pr_{0.3}Y_{0.2}O_{3-\delta}$ (BZPY)[22], $Ba_{0.5}Sr_{0.5}Co_{0.8}Fe_{0.2}O_{3-\delta}$ (BSCF)[15], $BaZr_{0.6}Co_{0.4}O_{3-\delta}$ (BZC)[23], $NdBa_{0.5}Sr_{0.5}Co_{1.5}Fe_{0.5}O_{5+\delta}$ (NBSCF)[24], $BaCo_{0.4}Fe_{0.4}Zr_{0.1}Y_{0.1}O_{3-\delta}$ (BCFZY0.1)[25], $PrBa_{0.5}Sr_{0.5}Co_{1.5}Fe_{0.5}O_{5+\delta}$ (PBSCF)[26,27], $Pr_{0.5}Ba_{0.5}(Co_{0.7}Fe_{0.25}W_{0.05})O_{3-\delta}$ (PBCFW)[28]. In addition, there are composite electrodes such as $Sm_{0.5}Sr_{0.5}CoO_{3-\delta}$ -$SmBaCo_2O_{5+\delta}$ (SSC-SBC)[29] and $LaNi_{0.6}Fe_{0.4}O_{3-\delta}$-$Sm_{0.5}Sr_{0.5}CoO_{3-\delta}$ (LNF-SSC)[30] showing decent electrochemical performances for IT-PCEC. However, there are concerns with these electrodes because alkaline earth elements of Ba and Sr have high affinity towards CO_2, which may lead to poisoning by CO_2 adsorption or even bulk reactions.[31–34] For instance, earlier study has shown that CO_2 adsorption on BSCF electrode may cause severe degradation in the cell performance.[35] In comparison, $PrNi_{0.5}Co_{0.5}O_{3-\delta}$ (PNC) is reported as a new promising triple conducting oxygen electrode.[17,18] However, how PNC would interact with CO_2 as well as moisture is not clear. In addition, earlier studies have shown that the electrical conductivity of

triple conducting materials of BCB, BSCF, BZC is lower than common oxygen electrodes like LSCF,[19,23,36] but the electrical conductivity of PNC electrode has not been investigated yet. Meanwhile the thermal expansion property of PNC is also unknown.

In this paper, the stability of PNC against H_2O and CO_2 is reported. The effect of H_2O and CO_2 on electrochemical behaviors of PNC oxygen electrode over BZCYYb4411 electrolyte is also studied and compared with PNC over $Ce_{0.9}Gd_{0.1}O_{2-\delta}$ (GDC) oxygen ion conducting electrolyte. Furthermore, H_2O and CO_2 adsorption behaviors on PNC oxygen electrode are studied by temperature-programmed desorption (TPD). In addition, other properties such as the total electrical conductivity and thermal expansion coefficient of PNC are reported in this paper to obtain a comprehensive understanding of the properties of this new electrode material.

2. Experimental

2.1. Powder synthesis

Both BZCYYb4411 and PNC powders were synthesized by Pechini method.[37] For BZCYYb4411, at first metal salts including $Ba(NO_3)_2$ (#A11305, Alfa Aesar, 99%), $ZrO(NO_3)_2 \cdot xH_2O$ (x=12 determined by calcination at 700°C in air for 2 h, #43224, Alfa Aesar, 99.9%), $Ce(NO_3)_3 \cdot 6H_2O$ (#11329, Alfa Aesar, 99.5%), $Y(NO_3)_3 \cdot 6H_2O$ (#12898, Alfa Aesar, 99.9%), $Yb(NO_3)_3 \cdot xH_2O$ (x=6 determined by calcination at 700°C in air for 2 h, #12901, Alfa Aesar, 99.9%) were dissolved in DI water according to stoichimetry ratio (100 ml water for 0.02 mole of target BZCYYb4411 electrolyte powder). Then polyethylene glycol (#25322-68-3, Scientific Polymer Products, Inc) and citric acid monohydrate (#22869, Alfa Aesar, 99.5%, Hygroscopic) were added to the salt solution with the ethylene glycol : citric acid : total metal ions molar ratio of 1.5:1.5:1. After that the solution was heat treated in a 2 L Pyrex glass beaker on a hotplate set temperature of ~540°C. A polymerized yellow gel was produced after water

was completely evaporated. Then the gel was continously heated on the hotplate for ~15 min and turned into a yellow porous mass. The product was cooled and hand ground to powder, which was then heat treated at 1300°C to form the phase. PNC powders were synthesized by the same technique. For PNC, the metal salts are $Pr(NO_3)_3 \cdot xH_2O$ (x=6 determined by calcination at 700°C in air for 2 h, #12909, Alfa Aesar, 99.9%), $Ni(NO_3)_2 \cdot 6H_2O$ (#A15540, Alfa Aesar, 98%), and $Co(NO_3)_2 \cdot 6H_2O$ (#239267, Sigma Aldrich, >= 98%). After the heating on the hot plate, calcination was carried out at 1000°C for 2 h to obtain the desired phase. In addition, $Ce_{0.9}Gd_{0.1}O_{2-\delta}$ (GDC) powder was synthesized by the glycine nitrate process (GNP). 0.0135 mole of $Ce(NO_3)_3 \cdot 6H_2O$ (#11329, Alfa Aesar, 99.5%) and 0.0015 mole of $Gd(NO_3)_3 \cdot 6H_2O$ (#12917, Alfa Aesar, 99.9%) metal salts and 0.025 mole of glycine ($C_2H_5NO_2$, #G8898, Sigma Aldrich, >=99+ %) were first dissolved in 30 g DI water. Then the solution was heat treated in a 2 L pyrex glass beaker on a hotplate set at ~540°C. After water was completely evaporated, auto-ignition occurred, and the light yellow fluffy powder obtained was calcined at 600°C for 2 h in a box furnace.

2.2. Symmetrical cells fabrication and electrochemical test

To fabricate proton conducting PNC/BZCYYb4411/PNC symmetrical cells, at first 0.2 g of BZCYYb4411 electrolyte powder with 0.5 wt.% NiO as sintering aid was dry pressed at 250 MPa into 10 mm green pellet. Sintering was carried out at 1450°C for 10 h in air under protective sintering condition in a box furnace (Three pellets were stacked up and covered with loose BZCYYb4411 powder both at the top and the bottom to prevent unwanted reaction with the alumina crucible). The pellet after sintering was found to be dense as shown in supplementary Fig. S1(a). After that the electrode slurry, made by mixing PNC powder and polymer binder solution (7 wt.% PVA in water) at weight ratio of 1:1, was manually brush painted onto both

sides of the BZCYYb4411 electrolyte followed by calcination at 1200°C for 2 h at the ramp rate of 2.5°C/min. The obtained electrolyte thickness was 0.58 mm, and the electrode area was 0.16 cm^2. The thickness of the electrode is ~35 μm. (The thickness of the electrode can be controlled by the slurry solid content and the number of layers of brush painting on the electrolyte.) Similarly, to fabricate oxygen ion conducting PNC/GDC/PNC symmetrical cells, GDC electrolyte was sintered at 1550°C for 5 h in air. The pellet after sintering was found to be dense as shown in supplementary Fig. S1(b). After sintering the PNC electrode was painted and fired also at 1200°C for 2 h. A PNC-GDC/GDC/PNC-GDC composite electrode symmetrical cell was also prepared in the same way. The weight ratio of PNC and GDC in the composite electrode is 70:30.

For electrochemical impedance spectroscopy (EIS) test of the symmetrical cells, silver paste was brush painted onto the electrodes of the symmetrical cells for current collection. The cell was placed into a sealed tube furnace (OTF-1200) to collect EIS from 650 to 450°C using a potentiostat (Gamry Interface 1000) with zero DC bias in frequency range of 10^6- 0.01 Hz. The AC amplitude is 1mA. Before taking EIS, all symmetrical cells were heated to 750°C in air and held for 12 h to stabilize them. After that EIS was taken in cylinder simulated air (Ultra Zero Grade, Airgas, <5 ppm H_2O and CO_2 by volume) at 650°C. To test the effect of H_2O, 3% H_2O (by volume; all gas compositions are by volume in this study) was introduced at 650°C by passing air through the water bubbler. After holding for 2-4 h to stabilize the system, EIS for the symmetrical cells was collected. To test the effect of both H_2O and CO_2, 5% CO_2 (controlled by mass flow controllers) were introduced to the simulated air after humidification at 650°C and held for 2 h. The testing sequence was similar for EIS measurements for 550 to 450°C. Note that for each of the temperature from 550 to 450°C, the symmetrical cells were always heated back up to 750°C in dry simulated air and held for 12 h or more to fully dehydrate the cells and remove

CO_2 adsorption. To test the effect of air dilution, 5% N_2 was added to the 3% humidified air at 450°C and held for 2 h for PNC/BZCYYb4411/PNC symmetrical cells and EIS was collected before and after air dilution by 5% N_2.

2.3. Materials characterization

Phase identification of the materials including as-synthesized BZCYYb4411 and PNC as well as those powders after exposure in simulated air with addition of 3% H_2O and 5% CO_2 for 46 h was carried out using different techniques such as X-ray diffraction (XRD, Siemens D5000 and Rigaku BD700535-01, Cu-K_α radiation, λ = 1.541874 Å), Raman spectroscopy (spectrometer Holo Spec f/l.8i, Kaiser Optical System; air-cooled Ar ion laser by Spectra Physics Model 177, 514 nm, 400 mW, spot size 10 μm), and Fourier Transform Infrared Spectroscopy (FTIR, Jasco ft/ir 4100). Density of the sintered pellets was determined by both dimension and Archimedes method. Microstructure and elemental composition of powders and sintered pellets were analyzed by a scanning electron microscope (SEM JEOL JSM-F100) fitted with energy dispersive X-ray spectroscopy (EDS).

The electrical conductivity of the PNC was measured by four probe method. To obtain the sample, at first PNC powder (2.1 g) was dry pressed at 125 MPa into a 10 mm green pellet. Sintering was carried out at 1100°C for 12h in air with the pellet buried in PNC loose powder. After that a rectangular bar was cut from the sintered PNC pellet by a diamond saw. The PNC bar was wrapped around by four silver wires. Silver paste was applied at the junction of silver wires and the bar followed by infrared lamp drying. The distance between two outer and two inner silver wires is ~6.1 mm and ~2.7 mm, respectively. The average width and height of the bar is ~1.3 mm and ~1.5 mm, respectively. Resistance between the two inner silver wires was measured by a potentiostat, with current passing through the outer wires and the voltage drop

measured across the two inner wires. The conductivity measurement was carried out in simulated air at temperature from 250 to 750°C. The relative density of the sintered sample is 78% by Archimedes method (~54% by the measurement of thickness and diameter). The bulk conductivity of the sample is calculated from the measured conductivity σ_m and total porosity ϵ using the following equation[38]:

(1)

In addition, to observe the effect of moisture on conductivity, a constant DC current of 50 mA was passed between two outer wires through the PNC bar at 450°C and the voltage was monitored with respect to time as moisture was introduced into and later removed from the simulated air.

The thermal expansion coefficient (TEC) measurement of PNC was carried out by both dilatometry and *in situ* XRD. For dilatometry, at first a PNC pellet was sintered at 1100°C for 12 h in air. After that experiment was carried out in a dilatometer (DIL801L) from room temperature to 800°C at the heating rate of 5°C/min in stagnant air. For *in situ* XRD, the experiment was carried out by Bruker AXS (Mo-K_α radiation, λ = 0.71073 Å) from room temperature to 900°C. A photo of the *in situ* XRD set up is given in Supplementary Fig. S2 where a thermocouple was touching the PNC powder encapsulated in thin (inside diameter of ~1 mm) quartz tube and the sample was heat treated by two halogen lamps. After the *in-situ* experiment, the diffraction patterns were plotted with respect to Mo-K_α radiation.

To analyze the H_2O and CO_2 adsorption behavior on PNC electrode and BZCYYb4411 electrolyte, at first the two powders were each exposed in simulated air with addition of 3% H_2O and 5% CO_2 at 450°C for 46 h. After that temperature programmed desorption (TPD) was carried out in an Omni Star gas analysis system (GSD 320). Before each experiment, each sample (~0.2

g) was flushed with dry argon at the flow rate of 20 cc/min at room temperature for 1 h to remove weakly adsorbed surface impurities. After that TPD was carried out from room temperature to 800°C at the heating rate of 5°C/min with the argon flow rate of 20 cc/min. The peaks (signals) were monitored with a quadruple mass spectrometer (MS, QMG 220).

3. Results and discussions

3.1. Phase identification

Supplementary Fig. S3(a) shows the diffraction patterns of BZCYYb4411 powders synthesized by Pechini method before and after calcination at 1300°C. As mentioned in experimental, before calcination, BZCYYb4411 is heat treated on a hotplate set at nominal temperature of 540°C to obtain $BaCO_3$ (PDF-04-015-3211) and doped ceria, as shown in Supplementary Fig. S3(a)-without calcination. (The real sample temperature should be somewhat lower.) After calcination at 1300°C, the diffraction patterns match with previous reports.[14,39] Its crystal structure can be indexed as cubic (*Pmm*) with a lattice parameter of 4.311 Å from XRD Rietveld refinement, as shown in Supplementary Fig. S3(b).

Fig. 1(a) shows the diffraction patterns of PNC powders also synthesized by Pechini method before and after calcination at 1000°C. Similar to the BZCYYb4411 electrolyte, before calcination, PNC is heat treated on a hotplate set at 540°C to obtain the sample that contains NiO (PDF-00-044-1159), Pr_6O_{11} (PDF-00-042-1121), $Pr_2NiO_{4+\delta}$ (PDF-04-016-4323) and partially formed PNC. After subsequent heat treatment at 1000°C, different phases react to form the PNC and the diffraction pattern matches with a previous report.[17] Its crystal structure can be indexed as orthorhombic with unit cell parameters of a = 5.382 Å, b = 7.624 Å, c = 5.409 Å from XRD Rietveld refinement, as shown in Fig. 1(b).

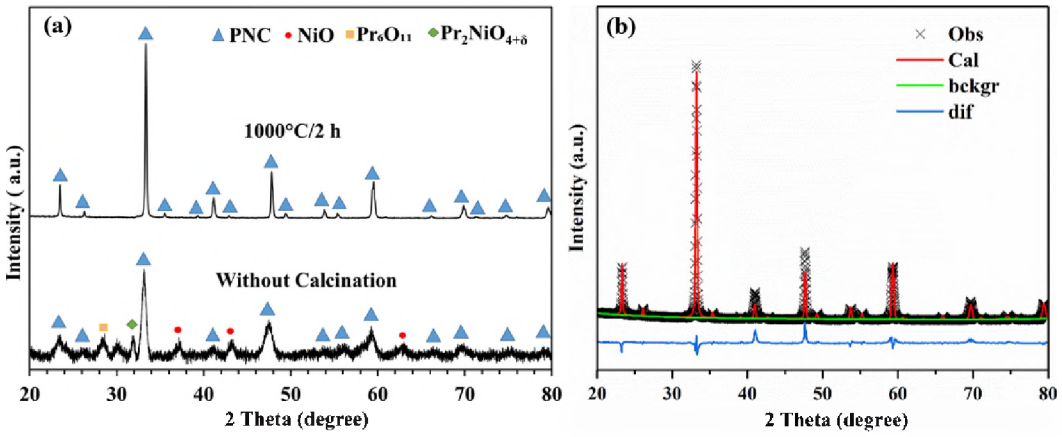

Figure 1: (a) Diffraction pattern of PNC powders synthesized by Pechini method before and after calcination at 1000°C for 2 h (b) XRD Rietveld refinement of PNC powder indexed to a *Pnma* orthorhombic structure with unit cell parameters of a = 5.382 Å, b = 7.624 Å, c = 5.409 Å.

3.2. Electrical conductivity of PNC

Fig. 2(a) shows the total conductivity at different temperatures (plotted in log scale vs 1000/T) for PNC in simulated air. PNC exhibits semiconducting behavior with conductivity increases from 210 S/cm at 250°C to 370 S/cm at 750°C. It shows a good linear relationship between ln(σT) and inverse temperature (see supplementary Fig.S4) between 250 and 750°C and the fitted activation energy is 10.9 kJ/mol or 0.11 eV. The measured conductivity is comparable to conventional oxygen electrodes such as $Pr_2NiO_{4+\delta}$, $La_{0.8}Sr_{0.2}MnO_{3-\delta}$ (LSM), $La_{0.6}Sr_{0.4}Co_{0.8}Fe_{0.2}O_{3-\delta}$ (LSCF), $La_{0.6}Sr_{0.2}Fe_{0.8}Ni_{0.2}O_{3-\delta}$, and $La_{0.6}Sr_{0.2}Fe_{0.8}Ni_{0.2}O_{3-\delta}$ (in the range of 100~500 S/cm at intermediate temperature 400-600°C) and much higher than several triple conducting electrodes such as $BaCe_{0.5}Bi_{0.5}O_{3-\delta}$, $BaZr_{0.6}Co_{0.4}O_{3-\delta}$, $BaZr_{0.1}Ce_{0.7}Y_{0.2-x}Co_xO_{3-\delta}$, $BaCo_{0.7}Fe_{0.7}Nb_{0.1}O_{3-\delta}$ (e.g., 0.1~10 S/cm at 600°C). [19,23,36,40,41] All these suggest PNC has adequate conductivity as an oxygen electrode for IT-PCEC.

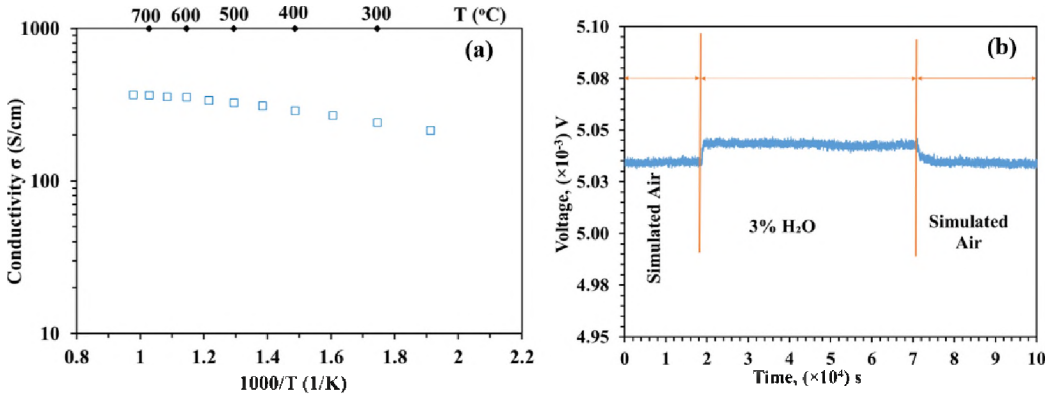

Figure 2: (a) Total electrical conductivity of PNC with respect to temperature in simulated air. (b) Voltage vs time for PNC sample bar at constant DC current of 50 mA at 450°C in simulated air when 3% moisture is introduced into and later removed from the air.

To understand the effect of moisture on electrical conductivity for PNC, a constant current of 50 mA is passed through the PNC sample bar at 450°C in simulated air. Fig. 2(b) shows the measured voltage (between the two inner electrodes on the sample bar) vs. time when 3% moisture is introduced into and later removed from the air. There is a slight increase of (~0.16%) of voltage when 3% moisture is introduced into the air. It seems reversible when the moisture is later removed. It's known for proton conductors such as BZCYYb4411, there are significant concentration of oxygen vacancy in the dry state. With moisture introduction, the oxygen vacancy gets filled up to form protons as below

$$H_2O + V_O^{\bullet\bullet} + O_O^x \leftrightarrow 2(OH)_O^{\bullet} \quad (2)$$

Because protons have higher mobility and lower activation energy than oxygen ions, conductivity often increases for proton conducting electrolytes upon hydration. The observation of slight increase in resistance and recovery for PNC when moisture is introduced indicates the

underlying defect reaction may *not* be filling up vacancy to form proton. Instead, it might be

$$H_2O + 2O_O^x + 2h^\bullet = 2OH_O^\bullet + 1/2\ O_2 \quad (3)$$

The mobility of proton $OH_O^\bullet$ might be lower than electron holes, leading to the slight reduction in conductivity with the introduction of 3% H_2O at 450°C. Such a hypothesis will be verified in future using techniques such as XPS or titration that can detect the valence state for the metal ions.

3.3. Thermal expansion co-efficient of PNC

Fig. 3(a) shows the thermal expansion curve obtained from dilatometry of a sintered PNC pellet from 100 to 800°C in air. From 100-800°C, the curve is linear with an average TEC of ~17.6×10^{-6}/K, which is high as an electrode material.[42] On the other hand, Fig. 4 shows the *in situ* XRD patterns of PNC powder from room temperature to 900°C. It shows the same diffraction pattern indicating no bulk phase change in that temperature range. The peaks are shifted towards lower angles at higher temperatures indicating lattice thermal expansion of PNC. Fig. 3(b) to (d) show the thermal expansion curves of lattice constants *a*, *b* and *c* for PNC from room temperature to 900°C. The fitted linear thermal expansion co-efficient of lattice constants *a, b* and *c* are found to be 18.5×10^{-6}, 23×10^{-6} and 13.8×10^{-6}/K, respectively. If taking the average of the three axes, the TEC from *in situ* XRD would be 18.43×10^{-6}/K, which is in good agreement with that of obtained by dilatometry. Nevertheless, due to the high TEC for PNC, there is a concern of delamination between electrolyte and electrode during thermal cycling especially to high temperatures since the TEC of barium cerate-based proton conducting electrolytes, such as $BaCe_{0.4}Zr_{0.4}Y_{0.2}O_{3-\delta}$, is 8.5~$10.9\times10^{-6}\ K^{-1}$.[43] As a result, PNC electrode should be fabricated at a very slow heating and cooling rate such as 2.5°C/min.

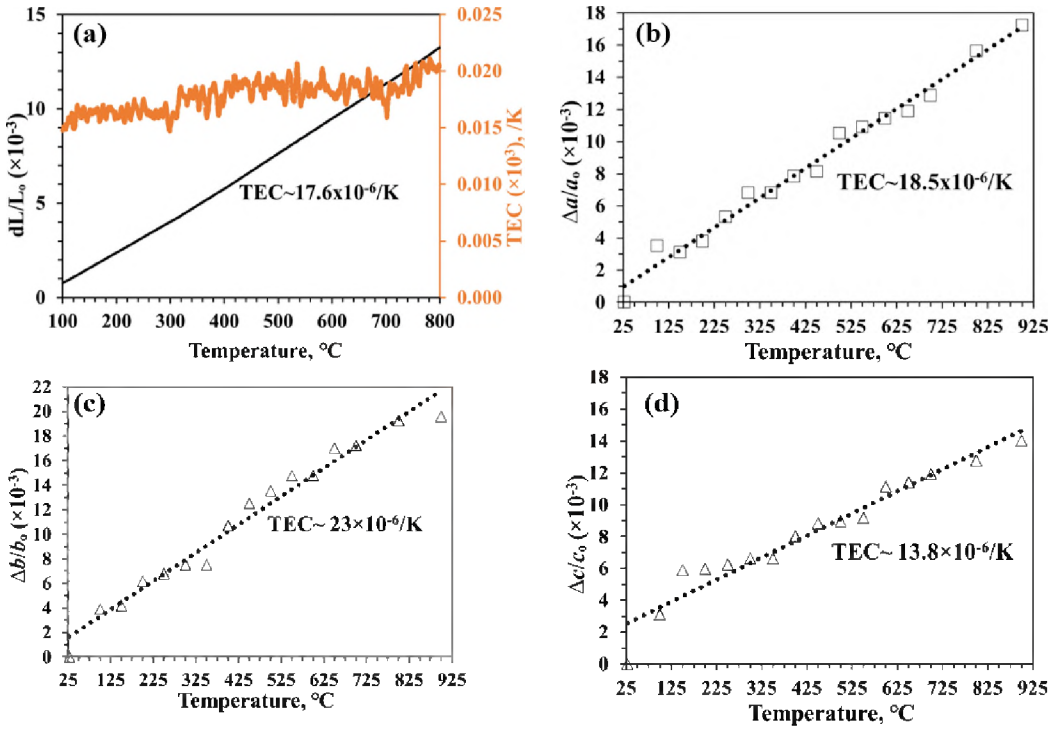

Figure 3: Thermal expansion curves of (a) sintered PNC pellet from 100 to 800°C in air obtained by dilatometry as well as lattice constants of (b) ***a***, (c) ***b***, and (d) ***c*** for PNC powder from room temperature to 900°C obtained by high temperature *in situ* XRD.

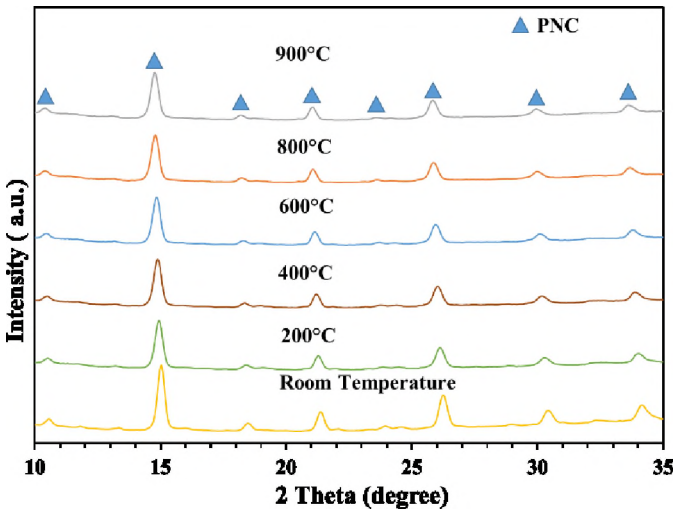

Figure 4: *In situ* XRD patterns of PNC powder from room temperature to 900°C (note the diffraction patterns were plotted with respect to Mo-K_α radiation).

3.4. Effect of H_2O and CO_2 on PNC electrode

3.4.1 Chemical stability of PNC and BZCYYb4411 against H_2O and CO_2

Fig. 5(a) shows the XRD of PNC powder before and after exposure to simulated air with addition of 3% H_2O and 5% CO_2. There is no change in XRD for the PNC powder after exposure indicating chemical stability against low percentage level of H_2O and CO_2. The chemical stability is also confirmed by FTIR as shown in Fig. 5(b). Unfortunately, to the best of our knowledge, there is no reliable thermochemical data about PNC or other Praseodymium compounds such as carbonates. Therefore, the thermodynamic calculations are not carried out. Nevertheless, literature suggests $Pr_2(CO_3)_3$, even after it is formed, decompose in air at ~400°C, which matches with the observed chemical stability for the PNC.[44] Similarly, BZCYYb4411 electrolyte powder is chemically stable against low percentage level of H_2O and CO_2, as shown in Fig. 5(c-d) and supplementary Fig. S5, respectively.

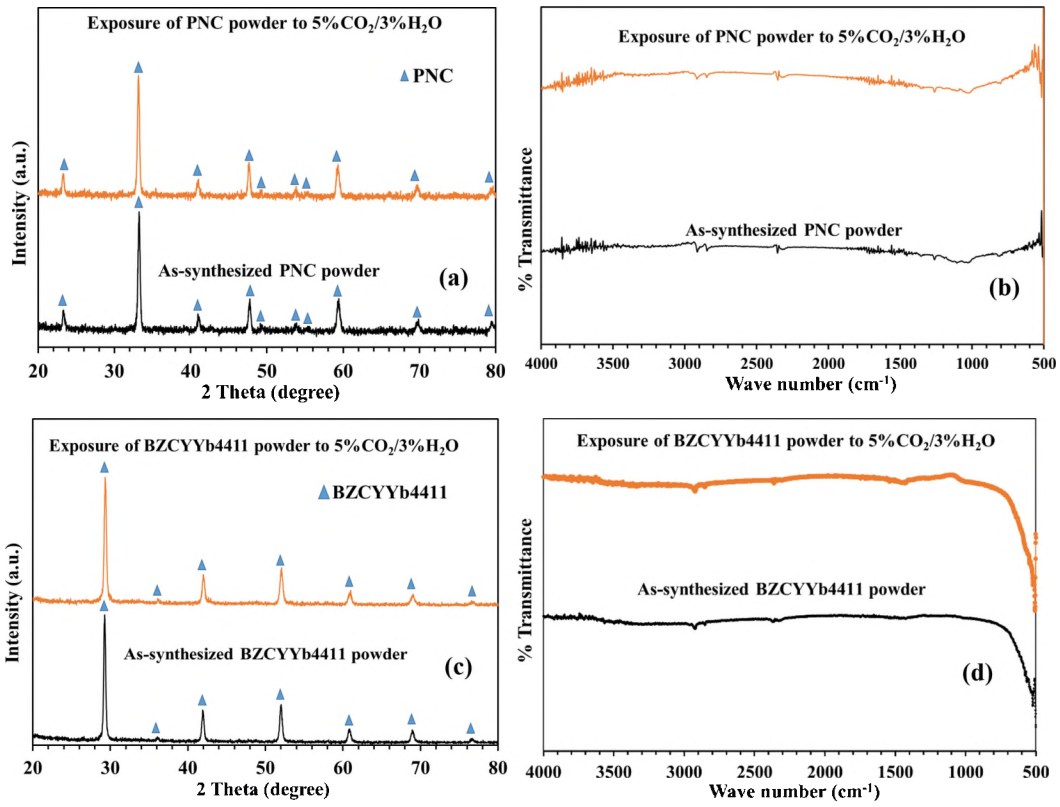

Figure 5: XRD patterns (a & c) and FTIR spectra (b & d) of PNC (a & b) and BZCYYb4411 (c & d) powders before and after exposure in simulated air with addition of 3% H_2O and 5% CO_2 at 450°C for 46 h.

3.4.2 Electrochemical response of PNC electrode to H_2O and CO_2

Fig. 6(a)-(c) show the impedance spectra of the PNC/BZCYYb4411/PNC symmetrical cell in simulated air without or with H_2O/CO_2 from 650 to 450°C. Compared with simulated air (according to the vendor, containing <5ppm H_2O and CO_2 by volume), ohmic resistance (R_0, the high frequency intercept in the impedance spectra) decreases when 3% H_2O is introduced, especially for 650 and 550°C. This is due to hydration of the BZCYYb4411 electrolyte and formation of proton $(OH)_O^{\bullet}$ from oxygen vacancy, which leads to higher bulk conductivity for

this proton conducting electrolyte. The low frequency loop becomes larger leading to the increase

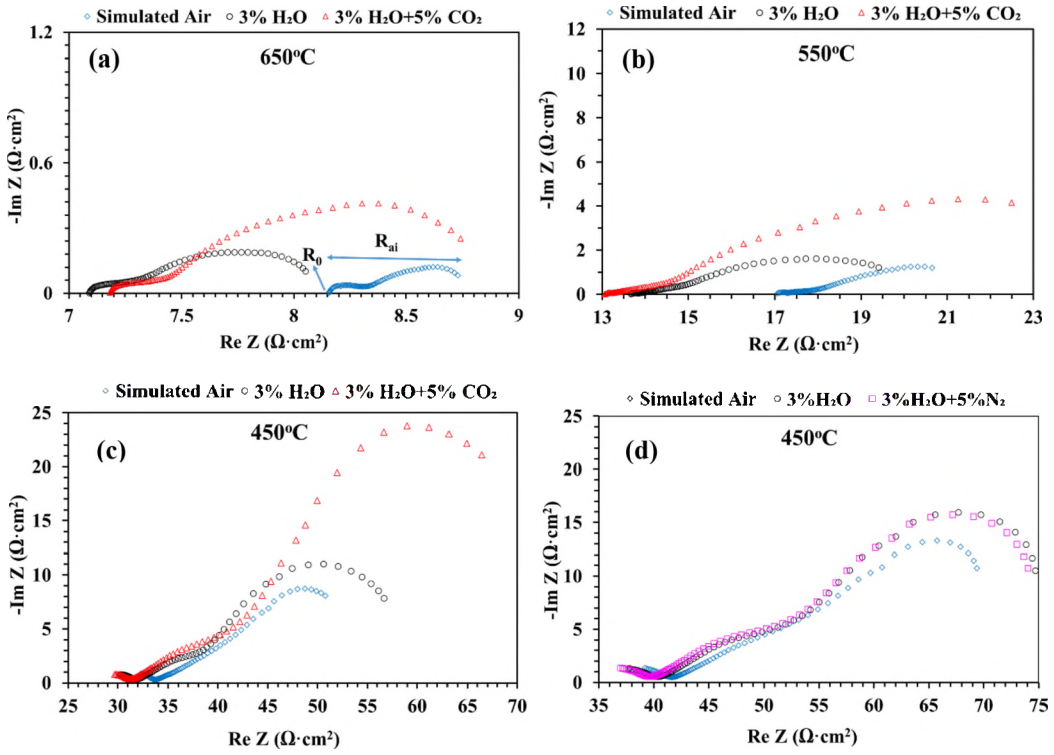

Figure 6: Plots of EIS for PNC/BZCYYb4411/PNC symmetrical cell in simulated air, 3% humidified air, and air with addition of 3% H_2O and 5% CO_2 at (a) 650, (b) 550, (c) 450°C; (d) EIS for air dilution test by 5% nitrogen for the same symmetrical cell at 450°C.

of apparent electrode interfacial resistance, R_{ai} (i.e., the direct difference between the high and low frequency intercept on the impedance spectra) by ~40-60%. This is probably due to the adsorption of H_2O molecules on the surface of either PNC electrode or BZCYYb4411 electrolyte reducing the active sites for O_2 adsorption and dissociation.

When 5% CO_2 is introduced to the humidified air, there is very small change in R_0. On the other hand, the high frequency loop remains the same, but the mid-to-low frequency loop gets larger leading to further increase of R_{ai}. To verify the change in impedance when 5% CO_2 is introduced is *not* due to air dilution effect, a separate experiment is carried out in which 5% N_2 (instead of 5% CO_2) is introduced to humidified air. Fig. 6(d) shows air dilution by 5% nitrogen does not cause any change in impedance, meaning this additional increase of R_{ai} with CO_2 introduction is a poisoning type of behavior and it is likely due to adsorption of CO_2 on either PNC or BZCYYb4411.

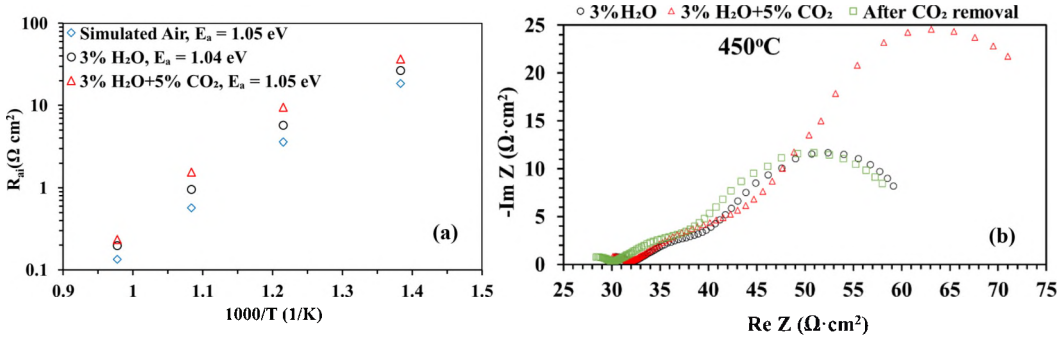

Figure 7: (a) Plot showing total apparent electrode interfacial resistance (R_{ai}) vs. inverse temperature for the PNC/BZCYYb4411/PNC symmetrical cell in simulated air, 3% humidified air and in air with 3% H_2O and 5% CO_2. The activation energy is also listed in the plot. (b) plot showing the reversible changes in EIS spectra when 5% CO_2 is introduced into and later removed from 3% humidified air for the PNC/BZCYYb4411/PNC symmetrical cell at 450°C.

Fig 7(a) shows the total apparent electrode interfacial resistance (R_{ai}) of PNC/BZCYYb4411/PNC symmetrical cell in simulated air, 3% humidified air and in air with 3% H_2O and 5% CO_2. By fitting the R_{ai} data into Arrhenius type equation, the activation energy

is found for three different conditions, which turned out to be almost the same (~1.04 eV). This means poisoning by H_2O/CO_2 adsorption does not change the nature of the rate limiting step for the oxygen electrode reaction.

In addition, CO_2 poisoning of the symmetrical cell is found to be recoverable at 450°C as shown in Fig. 7(b). The observations of almost no change in R_o and the reversible CO_2 poisoning for the symmetrical cell are consistent with the observed chemical stability for both PNC and BZCYYb4411 against CO_2 (see previous section). All these indicate the observed CO_2 poisoning is not caused by bulk reactions but also due to CO_2 adsorption on either PNC or BZCYYb4411.

To further distinguish if the poisoning by H_2O and CO_2 is due to their adsorption on the PNC electrode or the BZCYYb4411 electrolyte, the impedance spectra of another PNC symmetrical cell with an oxygen ion conducting electrolyte GDC, i.e., PNC/GDC/PNC is tested in simulated air without or with H_2O/CO_2 from 650 to 450°C (Supplementary Fig. S6). It should be noted that the cell performance is quite low in simulated air with high interfacial resistance, probably due to the microstructure of the cell not being optimized. (According to literature, the electrode polarization resistance of a symmetrical cell based on $PrNi_{0.6}Co_{0.4}O_{3-\delta}$ electrode over an $Ce_{0.8}Sm_{0.2}O_{1.9}$ (SDC) electrolyte was comparable to the current PNC/BZCYYb4411/PNC symmetrical cell,[45] indicating $PrNi_{0.5}Co_{0.5}O_{3-\delta}$ (close in stoichiometry to $PrNi_{0.6}Co_{0.4}O_{3-\delta}$) should be a decent electrode for oxygen ion-conducting electrochemical cells.) Nevertheless, at all three temperatures, when 3% H_2O is introduced into the simulated air, there is no change of R_o, which is expected since there would be no hydration for the oxygen ion ($V_o^{\bullet\bullet}$) conducting GDC electrolyte. Meanwhile, there is also no change of R_{ai} from 650 to 450°C with 3% H_2O introduction. When 5% CO_2 is further introduced to 3% humidified air, there is also no change of

R_o and R_{ai}. Similarly, even when using PNC-GDC composite electrode over the GDC electrolyte, there is still no H_2O and CO_2 poisoning for the PNC-GDC/GDC/PNC-GDC symmetrical cell as shown in Supplementary Fig. S7. All these observations indicate there is likely *no* obvious adsorption of H_2O and CO_2 on PNC (as well as GDC).

As a result, it can be hypothesized that poisoning from H_2O and CO_2 for PNC/BZCYYb4411/PNC proton conducting symmetrical cell is *not* caused by their adsorption on the PNC electrode. Instead, it is due to their adsorption on the BZCYYb4411 proton conducting electrolyte surface that blocks O_2 adsorption and dissociation inhibiting the oxygen electrode reaction ($O_2 + 4e^- + 4(OH)_O^{\bullet} \leftrightarrow 2O_O^x + 2H_2O$) at TPB as shown in Fig. 8.

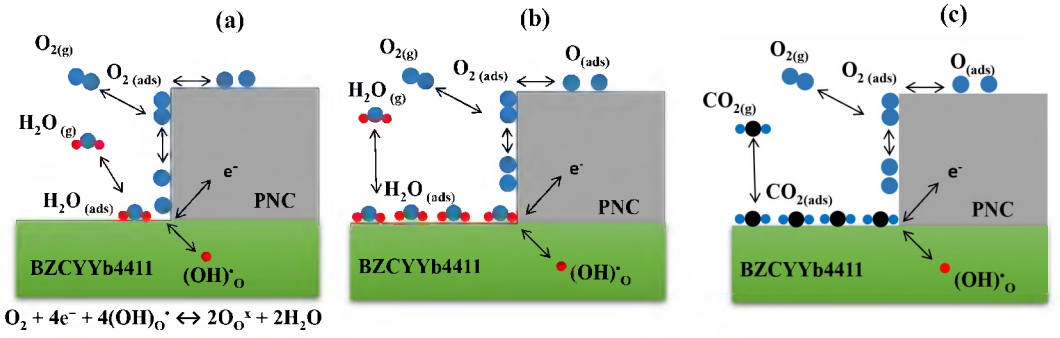

Figure 8: (a) Schematics showing oxygen electrode reaction at the TPB between PNC electrode, oxygen, and the BZCYYb4411 proton conducting electrolyte; (b and c) schematics showing preferred adsorption of (b) H_2O, and (c) CO_2 molecules over the BZCYYb4411 electrolyte, which would slow down the same electrode reaction at the TPB.

To prove this hypothesis, TPD has been carried out for both PNC and BZCYYb4411 powders. As mentioned in the experimental section, before TPD, each of the two powders has been exposed to simulated air with addition of 3% H_2O and 5% CO_2 at 450°C for 46 h to saturate

the surface. TPD of PNC shows *no* desorption peak for H_2O above 450°C and a very weak desorption peak for CO_2 at ~550°C as shown in Fig. 9(a) and (b). This indicates both H_2O and CO_2 have very weak adsorption over PNC surface at the cell test temperature above ~ 450°C. This is consistent with the absence of poisoning for PNC symmetrical cell over the GDC electrolyte (see Supplementary Fig. S6 and S7).

In comparison, TPD of BZCYYb4411 shows a very strong desorption peak for H_2O extends to ~650°C as shown in Fig. 9(c). This is expected due to the nature of the proton conducting

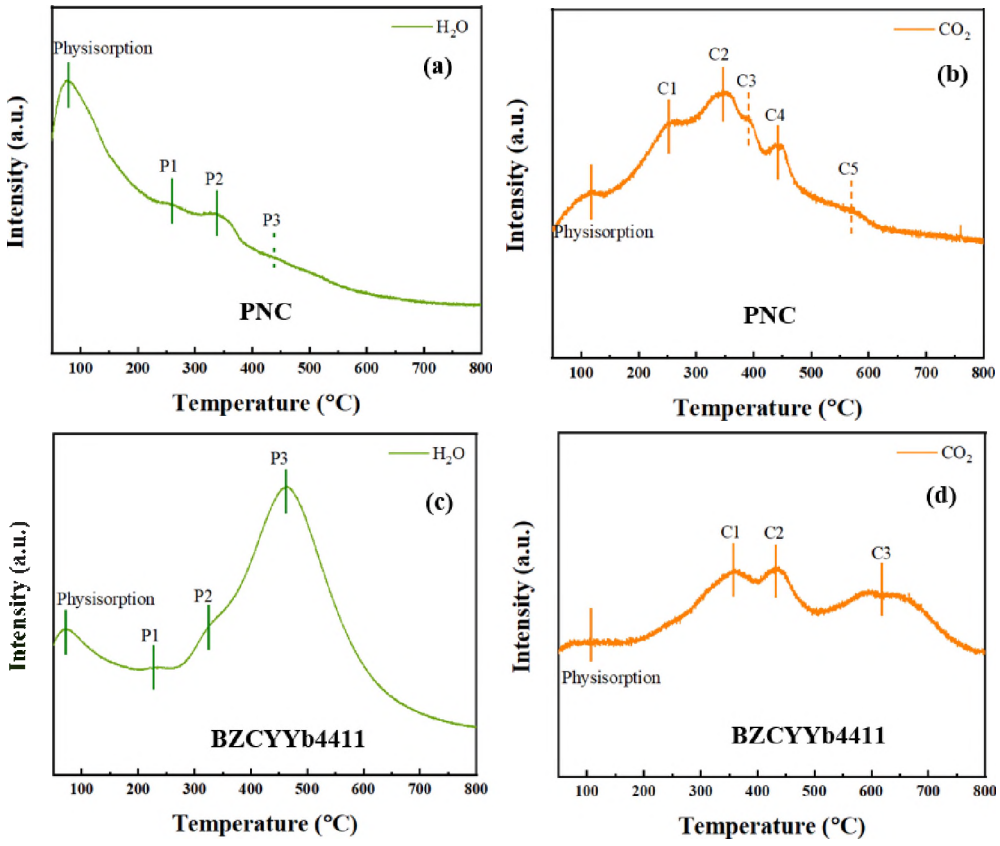

Figure 9: TPD profiles of H_2O (a and c) and CO_2 (b and d) for powders of PNC (a and b) and BZCYYb4411 (c and d), respectively. Note that before TPD, each of the two powders has been

exposed to simulated air with addition of 3% H_2O and 5% CO_2 at 450°C for 46 h to saturate the surface.

electrolyte. The strong adsorption of water over the electrolyte surface would inhibit the electrochemical half-cell reaction for oxygen electrode at the triple phase boundary, possibly by slowing down oxygen adsorption, dissociation, surface transport, and cause the observed increase in R_{ai} for the PNC/BZCYYb4411/PNC proton conducting symmetrical cell, as illustrated in Fig. 8(b).

As to CO_2, TPD shows a broad desorption peak from 500 to ~700°C for the BZCYYb4411 electrolyte as shown in Fig. 9(d). This is consistent with the earlier TPD studies on these types of Ba based proton conducting electrolyte.[4,46] Although this electrolyte has bulk stability against CO_2 (see section 3.4.1), the strong adsorption of CO_2 on the electrolyte surface above ~450°C explains the observed CO_2 poisoning behavior, as illustrated in Fig. 8(c).

4. Conclusions

This study shows PNC has adequate total electrical conductivity as an oxygen electrode and moisture does not have a significant effect on total electrical conductivity of PNC. Dilatometry and *in situ* XRD give similarly high TEC. While PNC is chemically stable against H_2O and CO_2, PNC symmetrical cell over proton conducting BZCYYb4411 electrolyte shows significant H_2O and CO_2 poisoning from 650 to 450°C. However, there is almost no H_2O and CO_2 poisoning for symmetrical cells with PNC electrode as well as PNC-GDC composite electrode over the oxygen ion conducting GDC electrolyte. As a result, it is hypothesized that H_2O and CO_2 poisoning for the PNC/BZCYYb4411/PNC symmetrical cell is caused by their adsorption on BZCYYb4411 proton conducting electrolyte, instead of adsorption on PNC. Such a hypothesis is supported by TPD. Future study aimed at detecting the metal valence state for

PNC under different conditions and characterizing the poisoning effect for practical concentration of CO_2 (~400 ppm) need to be carried out to fully understand the behavior of PNC oxygen electrode for protonic ceramic electrochemical cells.

CRediT authorship contribution statement

Md Shariful Islam Sozal: Conceptualization, Methodology, Investigation, Data curation, Writing – original draft. Wei Tang: Methodology. Suprabha Das: Methodology. Wenhao Li: Methodology. Andriy Durygin: Methodology. Vadym Drozd: Methodology. Cheng Zhang: Methodology. Borzooye Jafarizadeh: Methodology. Chunlei Wang: Methodology. Arvind Agarwal: Methodology. Dong Ding: Methodology. Zhe Cheng: Conceptualization, Supervision, Writing – review & editing.

Declaration of competing interest

The authors declare that they have no known competing financial interests or personal relationships that could have appeared to influence the work reported in this paper.

Acknowledgment

This research is supported by the National Science Foundation (Award No. NSF-1848305). WT and DD would like to thank the support by U.S. Department of Energy (USDOE), Office of Energy Efficiency and Renewable Energy (EERE), Hydrogen and Fuel Cell Technologies Office (HFTO) under DOE Idaho Operations Office under contract DE-AC07-05ID14517. The use of facilities at FIU Advanced Materials Engineering Research Institute (AMERI) is acknowledged.

References:

1. **Lu, C., An, S., Worrell, W. L., Vohs, J. M. & Gorte, R. J. Development of intermediate-temperature solid oxide fuel cells for direct utilization of hydrocarbon fuels. *Solid State Ionics* 175, 47–50 (2004).**

2. **Wachsman, E. & Lee, K. Lowering the Temperature of Solid Oxide Fuel Cells. *Science (80-.).* 334, 935–940 (2011).**

3. **Yamazaki, Y., Hernandez-sanchez, R. & Haile, S. M. High Total Proton Conductivity in Large-Grained Yttrium-Doped Barium Zirconate. *Chem. Mater.* 21, 2755–2762 (2009).**

4. **Guo, Y., Lin, Y., Ran, R. & Shao, Z. Zirconium doping effect on the performance of proton-conducting BaZryCe0.8−yY0.2O3−ı (0.0≤y≤0.8) for fuel cell applications. *J. Power Sources* 193, 400–407 (2009).**

5. **Yang, L. *et al.* Enhanced Sulfur and Coking Tolerance of a Mixed Ion Conductor for SOFCs: BaZr0.1Ce0.7Y0.2–xYbxO3–d. *Science (80-.).* 326, 126–129 (2009).**

6. **An, H. *et al.* A 5 × 5 cm2 protonic ceramic fuel cell with a power density of 1.3 W cm–2 at 600 °C. *Nat. Energy* 3, 870–875 (2018).**

7. **Duan, C., Huang, J., Sullivan, N. & O'Hayre, R. Proton-conducting oxides for energy conversion and storage. *Appl. Phys. Rev.* 7, (2020).**

8. **Vera, C. Y. R. *et al.* A mini-review on proton conduction of BaZrO 3 - based perovskite electrolytes. *J. Phys. Energy* 3, 1–13 (2021).**

9. **Duan, C. *et al.* Highly durable, coking and sulfur tolerant, fuel-flexible protonic ceramic fuel cells. *Springer Nat.* 557, 217–222 (2018).**

10. **Azad, A. K. *et al.* Improved mechanical strength , proton conductivity and**

power density in an ‘ all - protonic ’ ceramic fuel cell at intermediate temperature. *Sci. Rep.* **11, 1–10 (2021).**

11. An, H. *et al.* A 5 × 5 cm2 protonic ceramic fuel cell with a power density of 1.3 W cm–2 at 600 °C. 3, 870–875 (2018).

12. Vahidmohammadi, A. & Cheng, Z. Fundamentals of Synthesis, Sintering Issues, and Chemical Stability of BaZr0.1Ce0.7Y0.1Yb0.1O3-δ Proton Conducting Electrolyte for SOFCs. *J. ofThe Electrochem. Soc.* 162, F803–F811 (2015).

13. Sun, S., Awadallah, O. & Cheng, Z. Poisoning of Ni-Based anode for proton conducting SOFC by H 2 S , CO 2 , and H 2 O as fuel contaminants. *J. Power Sources* 378, 255–263 (2018).

14. Choi, S. *et al.* Exceptional power density and stability at intermediate temperatures in protonic ceramic fuel cells. *Nat. Energy* 3, 202–210 (2018).

15. Grimaud, A. *et al.* Hydration Properties and Rate Determining Steps of the Oxygen Reduction Reaction of Perovskite-Related Oxides as H+-SOFC Cathodes. *J. Electrochem. Soc.* 159, 683–694 (2012).

16. Sun, S. & Cheng, Z. Electrochemical Behaviors for Ag , LSCF and BSCF as Oxygen Electrodes for Proton Conducting IT-SOFC Electrochemical Behaviors for Ag , LSCF and BSCF as Oxygen Electrodes for Proton Conducting IT-SOFC. *J. Electrochem. Soc.* 164, F3104–F3113 (2017).

17. Ding, H. *et al.* Self-sustainable protonic ceramic electrochemical cells using a triple conducting electrode for hydrogen and power production. *Nat. Commun.* 11, (2020).

18. Bian, W. *et al.* Revitalizing interface in protonic ceramic cells by acid etch. *Nature* 604, 479–485 (2022).

19. Hui, Z. & Michele, P. Preparation, chemical stability, and electrical properties of Ba(Ce1-xBix)O3 (x ~ 0.0–0.5). *J. Mater. Chem.* 12, 3787–3791 (2002).

20. Tao, Z. *et al.* A novel single phase cathode material for a proton-conducting SOFC. *Electrochem. commun.* 11, 688–690 (2009).

21. Ding, H. & Xue, X. Proton conducting solid oxide fuel cells with layered PrBa0.5Sr0.5Co2O5+δ perovskite cathode. *Int. J. Hydrogen Energy* 35, 2486–2490 (2010).

22. Fabbri, E., Bi, L., Pergolesi, D. & Traversa, E. High-performance composite cathodes with tailored mixed conductivity for intermediate temperature solid oxide fuel cells using proton conducting electrolytes. *Energy Environ. Sci.* 4, 4984–4993 (2011).

23. Rao, Y. *et al.* Cobalt-doped BaZrO 3: A single phase air electrode material for reversible solid oxide cells. *Int. J. Hydrogen Energy* 37, 12522–12527 (2012).

24. Kim, J., Sengodan, S., Kwon, G., Ding, D. & Shin, J. Triple-Conducting Layered Perovskites as Cathode Materials for Proton-Conducting Solid Oxide Fuel Cells. *CHEMSUSCHEM Commun.* 7, 2811–2815 (2014).

25. Duan, C. *et al.* Readily processed protonic ceramic fuel cells with high performance at low temperatures. *Science (80-.).* 349, 1321–1326 (2015).

26. Choi, S. *et al.* Exceptional power density and stability at intermediate temperatures in protonic ceramic fuel cells. *Nat. Energy* 3, 202–210 (2018).

27. Im, S., Lee, J. H. & Ji, H. Il. PrBa0.5Sr0.5Co1.5Fe0.5O5+δ composite cathode in protonic ceramic fuel cells. *J. Korean Ceram. Soc.* 58, 351–358 (2021).

28. Tao, Z. *et al.* High-performing proton-conducting solid oxide fuel cells with triple-conducting cathode of Pr0.5Ba0.5(Co0.7Fe0.3)O3-δ tailored with W. *Int. J.*

Hydrogen Energy 47, 1947–1953 (2022).

29. Bu, Y. *et al.* A highly efficient composite cathode for proton-conducting solid oxide fuel cells. *J. Power Sources* 451, 227812 (2020).

30. Fu, M. *et al.* Fabrication and study of LaNi0.6Fe0.4O3-δ and Sm0.5Sr0.5CoO3-δ composite cathode for proton-conducting solid oxide fuel cells. *Sep. Purif. Technol.* 287, 120581 (2022).

31. Scholten, M. J. & Schoonman, J. Synthesis of strontium and barium cerate and their reaction with carbon dioxide. *Solid State Ionics* 61, 83–91 (1993).

32. Nornura, K., Ujihira, Y., Hayakawa, T. & C, K. T. CO 2 absorption properties and characterization of perovskite oxides, (Ba,Ca) (Co,Fe) 03_ d. *Appl. Catal. A Gen.* 137, 25–36 (1996).

33. Kharton, V. V *et al.* Perovskite-type oxides for high-temperature oxygen separation membranes. *J. Memb. Sci.* 163, 307–317 (1999).

34. Khromushin, I. V, Aksenova, T. I. & Zhotabaev, Z. R. Mechanism of gas–solid exchange processes for some perovskites. *Solid State Ionics* 162–163, 37–40 (2003).

35. Yan, A., Cheng, M., Dong, Y. & Yang, W. Investigation of a Ba0.5Sr0.5Co0.8Fe0.2O3_d based cathode IT-SOFC I. The effect of CO2 on the cell performance. *Appl. Catal. B Environ.* 66, 64–71 (2006).

36. Dailly, J. *et al.* Perovskite and A2MO4-type oxides as new cathode materials for protonic solid oxide fuel cells. *Electrochim. Acta* 55, 5847–5853 (2010).

37. Dumaisnil, K., Fasquelle, D., Mascot, M., Rolle, A. & Roussel, P. Synthesis and characterization of La0.6Sr0.4Co0.8Fe0.2O3 films for solid oxide fuel cell cathodes. *Thin Solid Films* 553, 89–92 (2014).

38. Juretschke, H. J., Landauer, R. & Swanson, J. A. Hall Effect and Conductivity in Porous Media. 27, 838–839 (1956).

39. Le, L. Q. *et al.* Proton-conducting ceramic fuel cells : Scale up and stack integration. *J. Power Sources* 482, 228868 (2021).

40. Yang, L., Wang, S., Lou, X. & Liu, M. Electrical conductivity and electrochemical performance of cobalt-doped BaZr0.1Ce0.7Y0.2O3-d cathode. *Int. J. Hydrogen Energy* 6, 2266–2270 (2010).

41. Lin, Y., Zhou, W., Sunarso, J., Ran, R. & Shao, Z. Characterization and evaluation of BaCo0.7Fe0.2Nb0.1O3-d as a cathode for proton-conducting solid oxide fuel cells. *Int. J. Hydrogen Energy* 37, 484–497 (2011).

42. Zhang, Y. *et al.* Thermal-expansion offset for high-performance fuel cell cathodes. *Nature* 591, 246–251 (2021).

43. Lyagaeva, Y. G., Medvedev, D. A., Demin, A. K., Tsiakaras, P. & Reznitskikh, O. G. Thermal expansion of materials in the barium cerate-zirconate system. *Phys. Solid State* 57, 285–289 (2015).

44. Sastry, R. L. N., Yoganarasimhan, S. R., Mehrotra, P. N. & Rao, C. N. R. Preparation, characterization and thermal decomposition of praseodymium, terbium and neodymium carbonates. *J. Inorg. Nucl. Chem.* 28, 1165–1177 (1966).

45. Huang, S., Lu, Q., Feng, S., Li, G. & Wang, C. PrNi0.6Co0.4O3-Ce0.8Sm 0.2O1.9 composite cathodes for intermediate temperature solid oxide fuel cells. *J. Power Sources* 199, 150–154 (2012).

46. Guo, Y., Ran, R. & Shao, Z. Fabrication and performance of a carbon dioxide-tolerant proton-conducting solid oxide fuel cells with a dual-layer electrolyte. *Int. J. Hydrogen Energy* 35, 10513–10521 (2010).